

NOTE

Simultaneous recording and marking of brain microstructures

To cite this article: Khalil B Ramadi *et al* 2020 *J. Neural Eng.* **17** 044001

View the [article online](#) for updates and enhancements.



The Department of Bioengineering at the University of Pittsburgh Swanson School of Engineering invites applications from accomplished individuals with a PhD or equivalent degree in bioengineering, biomedical engineering, or closely related disciplines for an open-rank, tenured/tenure-stream faculty position. We wish to recruit an individual with strong research accomplishments in Translational Bioengineering (i.e., leveraging basic science and engineering knowledge to develop innovative, translatable solutions impacting clinical practice and healthcare), with preference given to research focus on neuro-technologies, imaging, cardiovascular devices, and biomimetic and biorobotic design. It is expected that this individual will complement our current strengths in biomechanics, bioimaging, molecular, cellular, and systems engineering, medical product engineering, neural engineering, and tissue engineering and regenerative medicine. In addition, candidates must be committed to contributing to high quality education of a diverse student body at both the undergraduate and graduate levels.

[CLICK HERE FOR FURTHER DETAILS](#)

To ensure full consideration, applications must be received by June 30, 2019. However, applications will be reviewed as they are received. Early submission is highly encouraged.

Journal of Neural Engineering



NOTE

RECEIVED
2 June 2020

ACCEPTED FOR PUBLICATION
30 June 2020

PUBLISHED
23 July 2020

Simultaneous recording and marking of brain microstructures

Khalil B Ramadi^{1,2,9} , Canan Dagdeviren^{3,9} , Preksha Bhagchandani⁴ , Carlos Nunez-Lopez^{1,3,5} , Min Jung Kim⁶, Robert Langer^{1,2,7} , Ann M Graybiel⁶ and Michael J Cima^{1,8,10}

¹ Koch Institute for Integrative Cancer Research, Massachusetts Institute of Technology, Cambridge, MA 02139, United States of America
² Harvard–MIT Health Sciences and Technology Division, Massachusetts Institute of Technology, Cambridge, MA 02139, United States of America

³ Media Lab, Massachusetts Institute of Technology, Cambridge, MA 02139, United States of America

⁴ Department of Bioengineering, Massachusetts Institute of Technology, Cambridge, MA 02139, United States of America

⁵ IQS School of Engineering, Ramon Llull University, 08017, Barcelona, Spain

⁶ McGovern Institute for Brain Research and Department of Brain and Cognitive Sciences, Massachusetts Institute of Technology, Cambridge, MA 02139, United States of America

⁷ Department of Chemical Engineering, Massachusetts Institute of Technology, Cambridge, MA 02139, United States of America

⁸ Department of Materials Science, Massachusetts Institute of Technology, Cambridge, MA 02139, United States of America

⁹ These authors contributed equally to this work.

¹⁰ Author to whom any correspondence should be addressed.

E-mail: mjcima@mit.edu

Keywords: neural probe, probe localization, MRI, iron deposition, fiducial marker

Supplementary material for this article is available [online](#)

Abstract

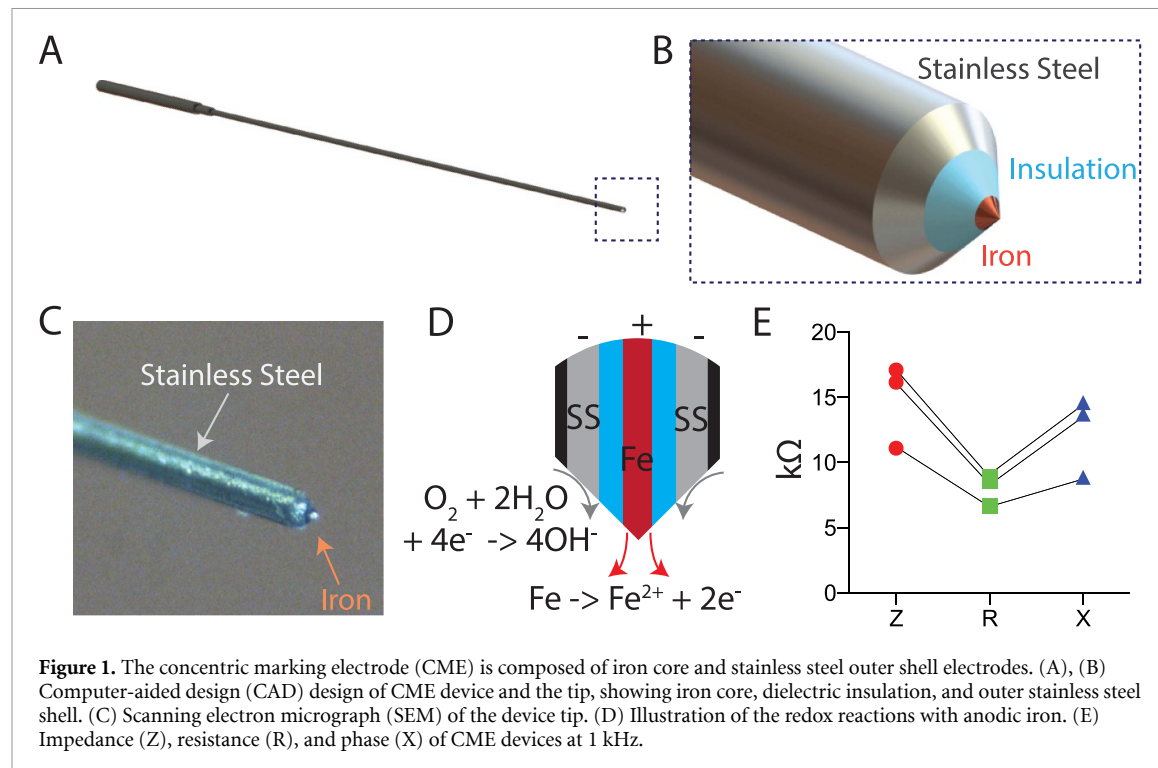
The vast majority of techniques to study the physiology of the nervous system involve inserting probes into the brain for stimulation, recording, or sampling. Research is increasingly uncovering the fine microstructure of the brain, each of its regions with dedicated functions. Accurate knowledge of the placement of probes interrogating these regions is critical. We have developed a customizable concentric marking electrode (CME) consisting of an iron core within a 125 μm -stainless steel (SS) sheath for co-localization of targeted regions in the brain. We used a dielectric layer stack of SiO_2 , Al_2O_3 , SiO_2 to electrically encapsulate the iron core and minimize exposure area to avoid significant increases in inflammatory response triggered by the probes. The CME can record multi-neuronal extracellular firing patterns. Appropriate electrical polarity of the iron and SS components controls the deposition of iron microdeposits on brain tissue. We show that *in vivo* labels by this method can be as small as 100 μm , visible via noninvasive magnetic resonance imaging (MRI) as well as post-mortem histology, and illustrate how deposit size can be tuned by varying stimulus parameters. We targeted the CA3 area of the hippocampus in adult rats and demonstrate that iron microdeposits are remarkably stable and persist up to 10 months post-deposition. Using a single probe for recording and marking avoids inaccuracies with re-insertion of separate probes and utilizes iron microdeposits as valuable fiducial markers *in vivo* and *ex vivo*.

1. Introduction

Neuroscience research is increasingly uncovering the functions of remarkably heterogeneous brain microstructures, even within small nuclei. Methods such as optogenetics, chemogenetics, and deep brain stimulation allow investigators to dissect highly compact and interconnected neural circuitry, using in most cases the insertion of probes into the brain [1]. Stereotactic surgical techniques, however, can be prone to error in targeting structures due to intra-animal variability, equipment, and operator experience [2–4]. This

is even true for some work on the human brain [5, 6]. Confirmation of probe placement in the appropriate region is of vital importance during invasive research or clinical neurosurgery.

Probe localization in experimental animal research has traditionally been done using post-mortem histology after conclusion of *in vivo* experiments. A nucleic acid stain can indicate regions with damage to neurons and glia, reflective of the presence of a foreign implant. However, brain tissue can be damaged or modified during histology, irreversibly losing valuable information about electrode



location [7]. Moreover, data may not be usable if the probe is found to have been inadequately placed, requiring discarding extensive and expensive experiments. Other techniques have been developed that depend on making lesions, infusing colored or fluorescent dyes, or depositing materials such as silver or iron [8–11]. Silver deposition requires applying a silver coating that can then be deposited once the probe is inserted. This coating, however, can increase gliosis upon insertion. This is particularly true for silver, which has been shown to be immunogenic [12]. Iron staining is attractive due to the advantage of being visible with magnetic resonance imaging (MRI) *in vivo* [9]. Indeed, MRI imaging of iron is the primary means of diagnosing neuroferritinopathy [13]. Iron is also readily taken up by neuroglia, preventing its diffusion or transfer away from the deposition site, unlike infused dye [9]. The inflammatory response to iron has also been shown to be limited to the immediately surrounding region and stable over time, unlike other foreign materials that could trigger a continuous neurodegenerative process. Studies have used stainless steel electrodes that can be corroded to deposit iron along with other stainless steel alloys of chromium, nickel, and manganese [10, 14].

Here we present the concentric marking electrode (CME), a custom microfabricated device, and illustrate its use for (1) *in vivo* extracellular multi-unit recordings and (2) placement of iron microdeposits as fiducial markers to evaluate probe position. Iron microdeposits are visible on both magnetic resonance imaging (MRI) and post-mortem histology. Microdeposit size can be directly controlled by stimulation parameters, and distinguished using MRI

up to 10 months after deposition. We also confirm chronic viability of the CME, illustrating that dielectric insulation of iron prevents any significant exacerbation of gliosis. Non-invasive detection and long-term durability of iron fiducial markers render them a versatile tool in neuroscience. CME couples neuronal recording and iron deposition capabilities into a single platform.

2. Results

2.1. CME fabrication and functionality

We constructed the CME on a microfabricated polyimide (PI) layer patterned using standard photolithography techniques (figures S1–S2 (available online at stacks.iop.org/JNE/17/044001/mmedia)). CME consists of a 25 μm iron core encapsulated with a dielectric layer stack of SiO_2 , Al_2O_3 , SiO_2 and encased within a 125 μm stainless steel outer shell (figures 1(A)–(C) and S3). Dielectric encapsulation using plasma-enhanced chemical vapor deposition and atomic layer deposition creates a well-defined tip. The probe design and dimensions allow for reliable, independent insertion into the brain without the need for an insertion shuttle or guide tube (figure S4) [15, 16].

Switching polarity of the iron core and stainless steel shell allowed us to regulate iron oxidation to deposit Fe^{2+} ions (figure 1(D)). The stainless steel cathode promotes bimetallic corrosion by reducing oxygen in the surrounding environment while the iron anode oxidizes to Fe^{2+} ions that mark the tissue [17, 18]. The driving force for this corrosion is the potential difference between electrodes as currents pass through stainless steel and iron. Corrosion

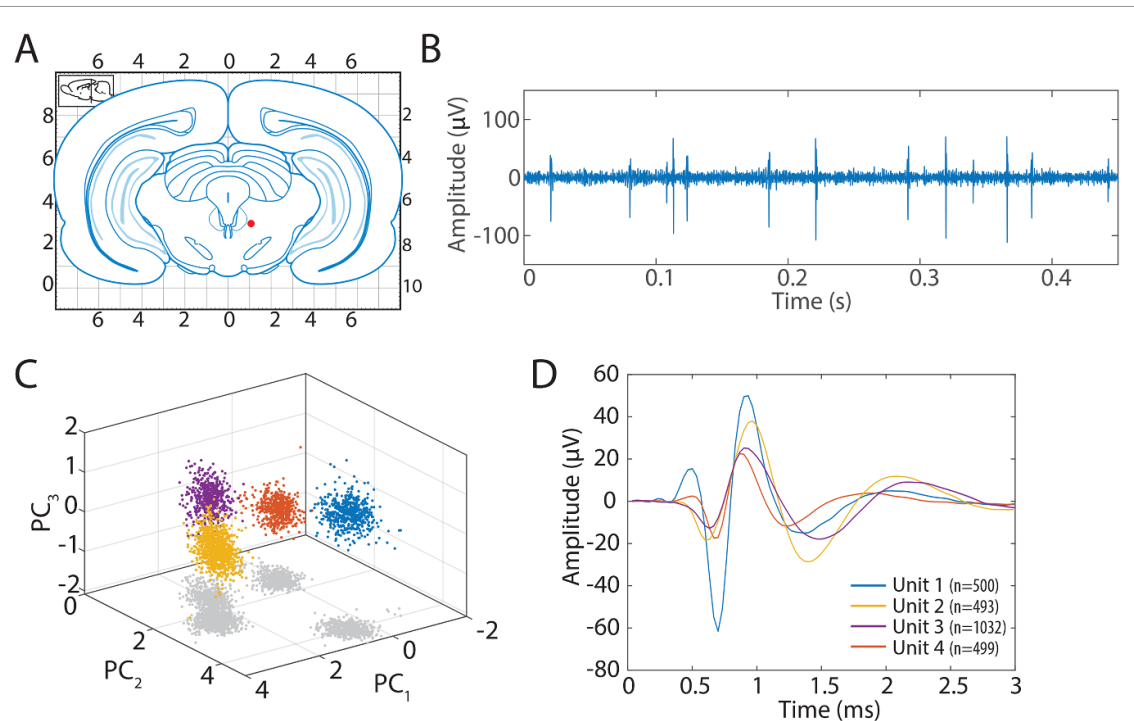


Figure 2. Multi-unit recording using CME. (A) Coronal section through rat brain (AP –5.88 mm) showing recording location in the mesencephalic reticular formation (mRF). (B) Representative electrophysiology signal recorded from the mRF. (C) Principal component analysis showing 4 distinct clusters. (D) Mean spike signal recorded corresponding to each unit, acquired over 70 s and shown with 95% confidence intervals (not visible).

is minimized when the current is eliminated. These sites can be visualized by MRI due to iron's paramagnetic properties. Switching the electrical polarity of the electrodes can halt iron oxidation. In this configuration, chromium within the stainless steel cathode oxidizes to form chromium oxide, a stable layer preventing iron corrosion. Multiple devices displayed similar electrical properties, reflecting the reliable fabrication process (Impedance 14.8 ± 3.2 kΩ at 1 kHz; figures 1(E) and S5).

2.2. Neural recording

We tested the CME recording capabilities by inserting it into the mesencephalic reticular formation (mRF) of an anesthetized rat (figure 2(A)). The mRF is known to play a role regulating locomotion, muscle tone, and sleep [19]. We used the iron core and stainless steel components as, respectively, the recording and reference electrodes for *in vivo* extracellular recording. The waveform features and spontaneous activity recorded were consistent with characteristics of mRF neurons previously reported [20, 21] (figure 2(B)). Both low and high-frequency components could be isolated by applying different bandpass filters on the obtained signal (figure S6). Neuronal discharges were detected from high-pass filtered data and were considered a valid spike when the signal-to-noise ratio was above 2. The CME could reliably record neuronal signals from multiple neurons with sufficient fidelity based on waveform features, which revealed four signal clusters corresponding to four

individual neurons according to principal component analysis (figures 2(C) and (D)).

2.3. Iron deposition

We next evaluated the ability of the CME to mark brain tissue. We inserted the probe and marked a series of loci along the length of the insertion trajectory targeting the CA3 of the hippocampus by using monophasic direct-current, galvanic electrical stimuli (Anodic iron; 30 μA for 20 s). We then reversed the polarity of the probe (cathodic iron), re-inserted the probe into the hippocampus in the contralateral hemisphere, and stimulated using identical parameters (figure 3(A)). One week later, iron microdeposits were visible on MRI on the side that was marked, while no deposits were detectable on the contralateral stimulated side (figure 3(B)). The electrical stimulation phase used here is significantly longer than conventional stimulation protocols [22]. Given this, the lack of iron deposition in the cathodic configuration illustrates the effectiveness of the chromium oxide layer in preventing iron corrosion from the stainless steel cathode.

We explored the ability of modulating the size of the marking loci to differentiate between multiple sites labeling adjacent structures. Deposition size is dependent on electrical charge, Q , which can be tuned by varying the stimulus pulse shape, according to:

$$Q = \int I_{stimulus} dt.$$

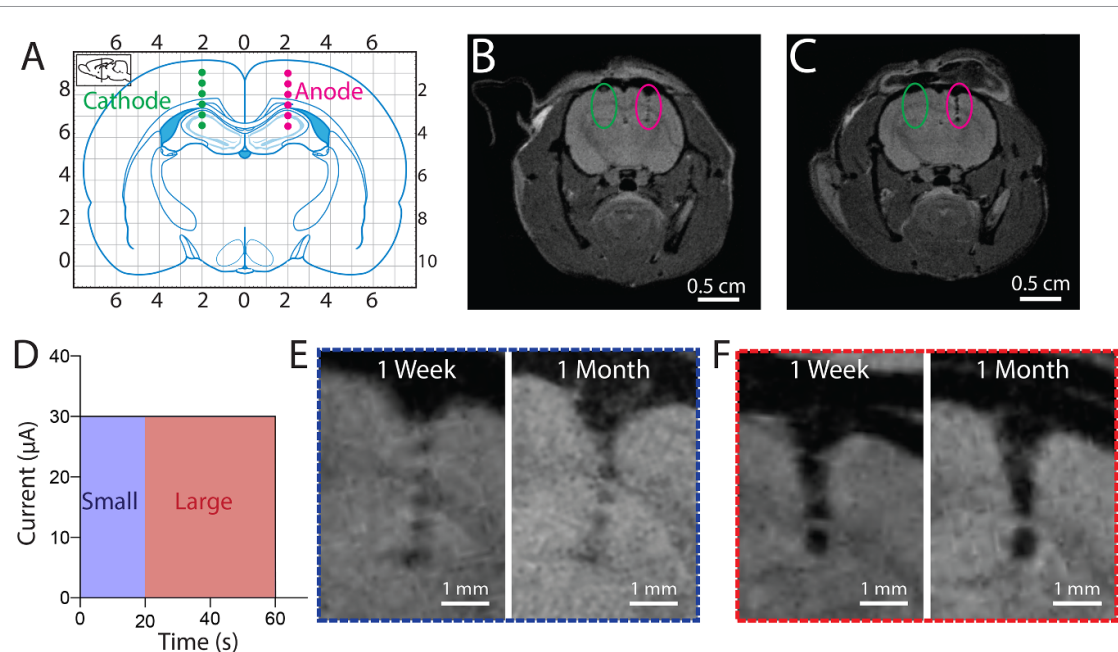


Figure 3. MR imaging of iron microdeposits. (A) Coronal section through rat brain (AP –2.3 mm) showing spots created bilaterally under anodic and cathodic iron conditions. (B), (C) MRI of rat brain showing small (B) and large (C) spots created under anodic conditions and lack of spots under cathodic conditions. (D) Stimulation parameters for small and large spot size cases. (E), (F) Expanded view of small (E) and large (F) iron deposits as imaged on MRI, 1 week and 1 month post-deposition.

Identical experiments were conducted stimulating at $30 \mu\text{A}$ (current density 43.2 kA m^{-2} , 4.23 A cm^{-2}) for 60 s per site (figure 3(D)). This created larger deposition marks that were visible on MRI (figures 3(C), (E) and (F)). Post-mortem histology of deposition sites created using $30 \mu\text{A}$ for 60 and 20 s, respectively, showed microdeposits to be $350 \mu\text{m}$ and $95 \mu\text{m}$ in diameter (figures 4(A)–(E) and S8). The different sizes of these microdeposits could also be detected by MRI. The measured size of each by MRI, however, is significantly larger than assessed with histology ($\sim 500 \mu\text{m}$ and $250 \mu\text{m}$ for larger and smaller microdeposits, respectively). This suggests that imaging artefact created by magnetic iron ions leads to a larger signal on MRI. This artefact, in fact, enables the visualization of smaller microdeposits on MRI.

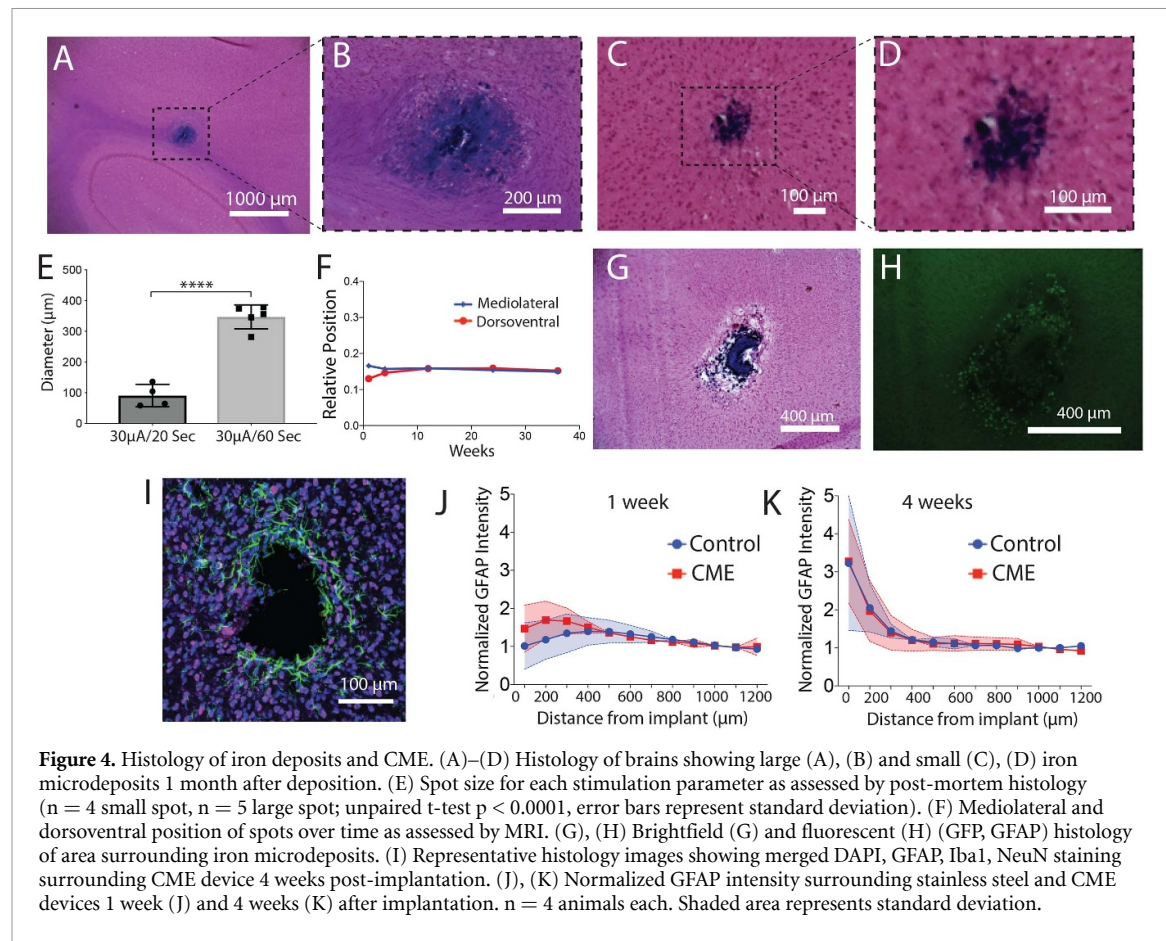
Small marked sites were present for up to 6 months, and thereafter were cleared from the brain and no longer visible on MRI (figure S7). The size of the deposition sites remained consistent on MRI measurements up to 3 months. Large marked sites remained visible up to 10 months post-marking. These were remarkably stable and did not move significantly from the original marking location (figure 4(F)). The hippocampus is implicated in memory formation and neurodegenerative disease [23]. It is known to be anatomically stable, with minimal shifts in placement over the course of rat adulthood [24]. The technique that we introduce here, however, could also be used to track developmental changes in brain structure with aging or in disease states [25].

2.4. Iron and CME biocompatibility

Iron can be pro-inflammatory. We assessed gliosis surrounding iron microdeposits and found no significant astrocyte staining in the surroundings 1 month after deposition (figures 4(G) and (H)). We also quantified the *in vivo* glial scar response to the chronic presence of an iron core. This is important as such probes may in some cases be chronically implanted. We implanted nonfunctional stainless steel shafts containing identical iron cores for up to 1 month and compared gliosis to stainless steel implants without iron (figure S9). We assessed inflammatory markers and neuronal viability at 3 d, 1 week, and 4 weeks after implantation. We found no significant difference in GFAP (astrocyte) staining between CME and control groups at any time point (figures 4(I)–(K) and S10). Astrocytes were observed to migrate to the probe over the course of the 4 weeks, as expected with any neural implant (figure S11). Dielectric insulation thus minimizes the area of exposed iron in the CME, limiting any enhanced glial response to the implant.

3. Discussion

These studies illustrate the potential for using iron microdeposits as fiducial markers for invasive neurosurgery. Co-registration of radiographic (CT) and magnetic resonance (MR) imaging has been proposed as a method to visualize chronic probe position *in vivo* with $625 \mu\text{m}$ precision [2, 26, 27]. We demonstrate that iron staining offers a simpler



approach to detect probe target with superior resolution ($100 \mu\text{m}$). Iron staining also offers the advantage of visualizing stimulation location after the probe has been removed from the brain, as well as on post-mortem histology.

The CME directly incorporates an iron core rather than relying on paramagnetic alloying metals of stainless steel, as previous iron staining techniques have done [10, 14]. This allows for a more reliable approach in tuning deposition size, based on theoretical modeling of iron oxidation. Using a single probe for recording and marking decreases inaccuracies inherent with insertion of separate probes for each purpose. In instances where deposition at multiple spots is performed, varying iron deposit size at each site can help to differentiate between these. The permanence of the iron spots is directly dependent on the size of the depositions. In this way, regions can be marked reversibly if there is no need for long-term chronic labeling. The stability of iron microdeposits could also be beneficial in examining long-term anatomic changes of the brain.

The microfabrication approach described here allows components to be readily interchanged. The stainless steel outer sheath, for example, can be switched with other metals or alloys without affecting probe functionality. Modular microfabrication techniques also allow for the addition of other modalities such as optic and fluidic interfacing [16, 28]. It is

likely that the CME can also be used for direct electrical stimulation, although this has not been confirmed in these studies. In this case, iron or stainless steel components of the probe can be used for monopolar stimulation, depending on the size of the region to be stimulated (Geometric Surface Area (GSA): $\text{GSA}_{\text{Fe}} = 694.3 \mu\text{m}^2$, $\text{GSA}_{\text{SS}} = 11107 \mu\text{m}^2$).

The CME exemplifies the use of an implantable probe with multiple functionalities. Some limitations do exist, however. Stimulation employed here for iron deposition is monophasic. Biphasic stimuli are commonly employed for electrical stimulation. This could result in some iron deposition, which could be a strength or limitation of the CME depending on whether this would be desired. While our studies describe iron deposition for $30 \mu\text{A}$ currents, brain stimulation protocols employ electrical currents an order of magnitude smaller ($\sim 5 \mu\text{A}$). This would also likely influence iron deposition. Future studies would investigate the evolution of iron deposits through histology beyond the 4 weeks shown here, and the potential for chronic neural recording during deposition. While no significant gliosis surrounding iron deposits was detected by histology, it is likely that they do interfere with local neuronal signaling. This will likely place an upper bound on the number of iron deposits that can be created in a specific area before interfering with neural physiology.

4. Conclusion

We report a concentric marking electrode that can label brain target areas as well as obtain multi-unit neuronal recordings. The size of iron microdeposits can be tuned by varying stimulation parameters. Sites are easily visualized *in vivo* and their *in vivo* stability is dependent on spot size. Deposition sites remain stable in position, allowing for repeated imaging of specific locations. The microfabrication approach described here allows components to be readily interchanged and used for multiple purposes. Given the variability encountered in stereotactic surgery, tools for the deposition of iron fiducial markers with dual recording capabilities are indispensable in the neuroscience toolkit.

5. Methods

5.1. Fabrication of CME

A silicon (Si) wafer was coated with a 50-nm-thick layer of poly(methyl methacrylate) (PMMA 495 A2) at 3000 rpm (PRM32, Headway Research, Garland, TX, USA) for 30s and baked on a hotplate at 180 °C for 2 min. A poly(puromellitic dianhydride-co-4,40-oxydianiline) amic acid solution (Millipore Sigma, Burlington, MA, USA) was then spun at 3000 rpm for 30 s and pre-cured on a hotplate at 250 °C for 1 min to form a 3.1 μm thick polyimide (PI) layer. This step was repeated three times to reach a ~9.3 μm thick layer of PI. The sample was then cured in a vacuum oven at 250 °C for 1 h. The walls of the PI template (depth of 3.1 μm) were formed by reactive ion etching (March RIE, Nordson, Westlake, OH, USA) through a pattern of photoresist (AZ 4620, Clariant, Muttenz, Switzerland) until the layer of PMMA was reached on the Si Wafer. The length of the PI template was set to 7 cm.

The tip of a 25 μm diameter thick iron rod was submerged into a polyvinyl alcohol (PVA) solution and dried at room temperature. A dielectric stack of silicon dioxide (SiO_2) (50 nm)/aluminum oxide (Al_2O_3) (10 nm)/ SiO_2 (50 nm) was deposited on the iron electrode via plasma enhanced chemical vapor deposition (PECVD, Plasmatherm System VII) and atomic layer deposition (ALD, Cambridge NanoTech Inc., Waltham, MA, USA) respectively to provide electrical insulation. The iron tip was then exposed by dissolving the protective layer of PVA in a water bath.

A 2 cm-thick stamp of polydimethylsiloxane (Sylgard 184), with a length and width of 8 and 2 cm, respectively, and a mixing ratio of 8.5:1.5 base to cross-linker, was used to pick up iron core gently and align it with the PI template under optical microscopy with the help of a mask aligner (Karl Suss Model MA4, Garching, Germany). A ~3 μm-thick layer of ultraviolet (UV) light-curable silicone adhesive (UV epoxy, LOCTITE 5055, Henkel Corp., Dusseldorf, Germany) coated the PI template, covered the iron core, and

allowed to cure inside a desiccator. The PI template with the iron core was immersed in a hot (85 °C) acetone bath to allow the sacrificial layer of PMMA to dissolve away. The epoxy-coated PI template was then physically free and could be retrieved from the acetone bath. The PI was aligned with the polished end of the stainless steel needle hole and along the needle hole by using a vacuum tweezer (Vacuum Pickup System, 115 V, Ted Pella Inc., Redding, CA, USA), which holds the template gently from the other end with a vacuum of 50.8 cmHg.

The assembled device with the exposed iron core was placed into the polisher holder, angled to 45° and positioned until the tip touched the polishing film (8 inch diameter aluminum oxide, Al_2O_3 , polishing film, ULTRATEC Manufacturing Inc., Santa Ana, CA, USA). Device was polished for 2 h with a lap speed of 250 rpm. It was then immersed into water in an ultrasonic cleaner (KENDAL, Model CD-3800A) for ~3 min to clean the remaining residues.

The electrical connection to the electrode was made via a metal pin (Conn Recept Pin, Mill-Max Manufacturing Corp, Oyster Bay, NY, USA; 7.62 mm length, ~0.38 mm to ~0.56 mm accepting pin diameter, 0.94 mm mounting hole diameter, 0.79 mm pin hole diameter, 1.04 mm flange diameter, 0.46 mm tail diameter, 3.81 mm socket depth). The UV epoxy was then used to fill the gap between the PI template and the needle hole via vacuum tube, sucking from one end and filling with epoxy on the other end of the needle. This fabrication and assembly approach enables modification of CME length according to the desired application.

5.2. Surgeries and animal procedures

F344 (SAS Fischer) rats were purchased from Charles River laboratories and maintained under standard 12 h light/dark cycles. Rats underwent one of three distinct surgeries: (1) electrophysiological recording, (2) Iron deposition, and (3) CME biocompatibility testing. All animal protocols were approved by the MIT Committee for Animal Care.

5.2.1. Biocompatibility assessment.

Caps were micromachined on a CNC mill (Micro Machining Center, Cameron Micro Drill Presses, Sonora, CA, USA). A CME or sham tip were inserted into each cap. CME tips contained the iron core while sham tips were composed of only the stainless steel outer core. Each of twelve rats underwent bilateral craniotomy and had a device implanted on either side of the cortex. Briefly, the animals were placed in a stereotactic frame, and a midline incision made to expose the skull, followed by bilateral burr hole drilling using a dental drill with 1 mm drill bits (Meisinger GmbH, Germany). The burr holes were located approximately 3 mm posterior from the bregma and 2 mm on either side of the midline.

The devices were then inserted, the caps cemented to the skull using C&B Metabond adhesive (Parkell Inc. Edgewood, NY, USA) and Orthojet dental cement (Lange Dental, Wheeling, IL, USA), and the incision was closed using 5–0 monofilament non-resorbable suture. No bone-screw was used. Animals displaying extensive post-operative morbidity more than 72 h post-surgery were euthanized and not further used in the study. At 3, 7, and 28 d post-implantation, 4 animals were euthanized and processed as described below (Histology).

5.2.2. Electrophysiology recording and spike sorting.

The animal underwent unilateral craniotomy as described above and had the CME acutely inserted in the mesencephalic reticular formation (stereotactic coordinates –5.88AP, 1 mm ML, –7.0 mm DV from brain surface). The iron core was used as recording electrode and stainless steel shell as a reference. Each ending was prepared with a millmax male pin. The pins were connected to a recording channel and a reference channel of 27-channel preamplifier (HS-27 headstage, Neuralynx, Bozeman, MT, USA), respectively. Output signal was acquired with an input range of $\pm 200 \mu\text{V}$, filtered between 0.1 Hz and 9.0 kHz, digitized at 30 kHz, and stored on a PC through digital Lynx system (Neuralynx). To obtain spike activities, bandpass filtered (600 Hz–3 kHz) signal was extracted to capture entire spike waveform and sorted out using Plexon offline sorter (Plexon, Dallas, TX, USA) based on waveform features.

5.2.3. Iron deposition.

Four animals underwent bilateral craniotomy as described above and had the CME acutely inserted in the CA3 of the hippocampus (–2.3 mm AP, 2 mm ML, –3.5 mm to –1 mm DV). CME was lowered to DV –3.5 mm, constant current electrical stimulation turned on for 20 or 60 s for small or large iron deposition, respectively, ($30 \mu\text{A}$, anodic iron), left in place for 60 s, and slowly retracted by 0.5 mm where it was turned on once more. The process was repeated 6 times. This process was repeated on the contralateral side with electrical polarity reversed (cathodic iron). Two animals were euthanized one month after surgery.

5.3. MRI methods

Magnetic resonance imaging was used to visualize iron deposits. MRI was performed using a Varian 7T/310/ASR-whole rat MRI system (Varian/Agilent) equipped with a 63 mm quadrature coil. The animal was anesthetized using 1%–2% isoflurane throughout the entire imaging session, and placed in a small, plastic sled that slid securely into the bore of the magnet. Hot air was delivered throughout the imaging session to provide heat. A series of low-resolution SCOUT scans were made to identify anatomical structures and determine the ideal locations

of imaging planes. 14 high resolution fast spin echo sequence (FSEMS) axial slice images were taken with the following parameters: TR/TE = 2000/12.85 ms, echo train length (ETL) = 4, kzero = 3, 512×512 matrix, field of view (FOV) = $50 \times 50 \text{ mm}^2$, interleaved number of slices = 30, slice thickness = 0.5 mm (no gap), number of averages = 2. Images were taken in 14 block slices in between respirations, and averaged over 2 images. Scans were collected with respiratory gating (PC-SAM version 6.26, SA Instruments Inc., Stony Brook, NY, USA) to avoid confounding noise due to chest movement. Images were converted to DICOM format for analysis purposes. Animals were scanned at 1 week ($n = 4$), 1 month ($n = 4$), 3 months ($n = 2$), 6 months ($n = 2$), 10 months ($n = 1$), and 12 months ($n = 1$).

5.4. Iron deposit position tracking

Tracking of deposit position was tracked by manual analysis of coronal brain sections obtained from MRI-generated DICOM images. Midlines were defined based on the anatomical landmarks. The position of the lowermost iron deposit from the midline and top of brain was measured. To account for inevitable variations in animal placement during each scan, this distance was represented as a fraction of the overall height and width of the brain in the same image.

5.5. Histology

Animals were euthanized using Carbon Dioxide asphyxiation. Each animal consequently underwent cardiac perfusion of 60 ml 1× Phosphate Buffered Saline (PBS) solution (Corning Inc. Corning, NY, USA), followed by 60 ml 4% Paraformaldehyde (PFA) solution (Alfa Aesar, Ward Hill, MA, USA). The head was then removed and immersed in 4% PFA for 48 h. The implanted devices were extracted, and the brain removed and placed in 4% PFA overnight, and consequently in sinking solutions of increasing sucrose (Amresco Inc. Solon, OH, USA) concentration (10%, 20%, 30%, overnight or until brain sinks). The brain was embedded in frozen tissue embedding medium (Sakura Finetek USA, Torrance, CA, USA), and frozen in a liquid nitrogen bath. 20 μm transverse slices were cut using a Leica CM1900 cryostat (Leica Biosystems Inc. Buffalo Grove, USA), starting at the top of the brain, and descending 80 mm, past the tips of the previously implanted devices. Slides were stored at -80°C .

Slides from brains in which iron was deposited were stained with standard Iron Stain kit protocols (Millipore Sigma). Biocompatibility test slides were stained for astrocytes (Glial fibrillary acidic protein (GFAP)), microglia (Iba1), neurons (NeuN), and nuclei (Hochst/DAPI) removed from -80°C , placed at room temperature for 20 min, and rehydrated by placing in a 1 × PBS solution for 10 min. Samples were then immersed in blocking solution

(5% Bovine Serum Albumin (BSA) (Rockland, Limerick, PA, USA)) for 50 min, followed by overnight incubation at 4°C in primary antibody incubation solution. (1:100 mouse anti-GFAPx488 Alexafluor, 1:300 rabbit anti-NeuN, (EMD Millipore, Billerica, MA, USA), 1:300 goat anti-Iba1 (Abcam, Cambridge, MA, USA) in incubation buffer (1% BSA, 1% normal Dk serum, 0.3% Triton X-100, 0.1% Sodium Azide). Slides were rinsed 3 times in 1× PBS (0.1% Tween), and incubated in secondary antibody solution (1:300 Dk × Gt × Cy3 & 1:300 Dk × Rb × Dy650 (Abcam) for 40 min. Samples were rinsed 3 times in 1× PBS, and incubated with Hochst solution ($0.1 \mu\text{g ml}^{-1}$) for 5 min, followed by mounting in gold antifade mounting medium (Life Technologies, Carlsbad, CA, USA).

5.6. Histology image analysis

Iron-stained slides were imaged using brightfield microscopy. Iron spots were measured using ImageJ software. Biocompatibility images were taken using fluorescence microscopy (EVOS FL Auto, Life Technologies, Grand Island, NY, USA) and analyzed with custom MATLAB scripts kindly provided by Dr. Jeffrey Capadona of Case Western Reserve University [29]. These scripts define the boundary of the hole created by the CME implantation, and then sum the intensity of each of the 4 stains in 2 mm radial increments from the hole boundary, up to 1100 mm away from the edge of the hole. For the purposes of data analysis, GFAP intensities were used as the primary indicator for the extent of glial scar formation around the implant. The intensities were then averaged into 50 mm bins and normalized such that the intensity 900–1100 mm away was equal to 1.

Acknowledgments

We thank Wei Huang of the Animal Imaging Core Facility at the Koch Institute for Integrative Cancer Research for her assistance with MRI. This work is supported by the US National Institutes of Health, National Institute of Biomedical Imaging and Bioengineering (R01 EB016101 to RL, AMG, and MJC), and in part by the National Cancer Institute (P30-CA14051 to the Koch Institute Core). The data sets, materials, and analysis generated during the current study are available from the corresponding author on reasonable request.

Author contributions

K.B.R., C.D., R.L., A.M.G., M.J.C. designed research; K.B.R., C.D., P.B., C.N.L., M.J.K. performed research; K.B.R., C.D., P.B., C.N.L., M.J.K. analyzed data; K.B.R., C.D., R.L., A.M.G., M.J.C. wrote the paper.

Conflict of interest

Authors declare no competing interests

ORCID iDs

- Khalil B Ramadi  <https://orcid.org/0000-0002-5864-2386>
- Canan Dagdeviren  <https://orcid.org/0000-0002-2032-792X>
- Preksha Bhagchandani  <https://orcid.org/0000-0001-9708-5896>
- Carlos Nunez-Lopez  <https://orcid.org/0000-0001-9859-8562>
- Robert Langer  <https://orcid.org/0000-0003-4255-0492>
- Ann M Graybiel  <https://orcid.org/0000-0002-4326-7720>
- Michael J Cima  <https://orcid.org/0000-0003-2379-6139>

References

- [1] Frank J A, Antonini M-J and Anikeeva P 2019 Next-generation interfaces for studying neural function *Nat. Biotechnol.* **37** 1013–23
- [2] Rangarajan J R et al 2016 Image-based in vivo assessment of targeting accuracy of stereotactic brain surgery in experimental rodent models *Sci. Rep.* **6** 38058
- [3] Whishaw I Q, Cioe J D, Previsich N and Kolb B 1977 The variability of the interaural line vs the stability of bregma in rat stereotaxic surgery *Physiol. Behav.* **19** 719–22
- [4] Tan S et al 2010 Experimental deep brain stimulation in animal models *Neurosurgery* **67** 1073–9
- [5] Duchin Y et al 2018 Patient-specific anatomical model for deep brain stimulation based on 7 Tesla MRI *Plos One* **13** e0201469
- [6] Li Z, Zhang J-G, Ye Y and Li X 2016 Review on factors affecting targeting accuracy of deep brain stimulation electrode implantation between 2001 and 2015 *Stereotact Funct. Neurosurg.* **94** 351–62
- [7] Fischer A H, Jacobson K A, Rose J and Zeller R 2008 Cryosectioning tissues *Cold Spring Harb. Protocols* **2008** pdb.prot4991
- [8] Spinelli D N 1975 Silver tipped metal microelectrodes- a new method for recording and staining single neurones *Brain Res.* **91** 271–5
- [9] Fung S H, Burstein D and Born R T 1998 In vivo microelectrode track reconstruction using magnetic resonance imaging *J. Neurosci. Methods* **80** 215–24
- [10] Green J D 1958 A simple microelectrode for recording from the central nervous system *Nature* **182** 962
- [11] Streeter K A et al 2017 Coupling multielectrode array recordings with silver labeling of recording sites to study cervical spinal network connectivity *J. Neurophysiol.* **117** 1014–29
- [12] Croes M et al 2018 Antibacterial and immunogenic behavior of silver coatings on additively manufactured porous titanium *Acta Biomater.* **81** 315–27
- [13] Ohta E and Takiyama Y 2012 MRI findings in neuroferritinopathy *Neurol. Res. Int.* **2012** 197438
- [14] Brown K T and Tasaki K 1961 Localization of electrical activity in the cat retina by an electrode marking method *J. Physiol.* **158** 281–95
- [15] Ramadi K B and Cima M J 2019 Materials and devices for micro-invasive neural interfacing *MRS Adv.* **4** 2805–16
- [16] Ramadi K B et al 2018 Focal, remote-controlled, chronic chemical modulation of brain microstructures *Proc. Natl. Acad. Sci.* **10** 7254–9
- [17] Simões A et al 2007 Use of SVET and SECM to study the galvanic corrosion of an iron–zinc cell *Corrosion Science* **49** 726–39

- [18] Souto R, Gonzalez-Garcia Y, Bastos A C and Simões A 2007 Investigating corrosion processes in the micrometric range: a SVET study of the galvanic corrosion of zinc coupled with iron *Corrosion Science* **49** 4568–80
- [19] Zaaimi B, Soteropoulos D S, Fisher K M, Riddle C N and Baker S N 2018 Classification of neurons in the primate reticular formation and changes after recovery from pyramidal tract lesion *J. Neurosci.* **38** 6190–206
- [20] MacGregor R J, Prieto-Diaz R, Miller S W and Groves P M 1973 Statistical properties of neurons in the rat mesencephalic reticular formation *Brain Res.* **64** 167–87
- [21] Maeda H and Mogenson G J 1982 Effects of peripheral stimulation on the activity of neurons in the ventral tegmental area, substantia nigra and midbrain reticular formation of rats *Brain Res. Bull.* **8** 7–14
- [22] Cogan S F 2008 Neural stimulation and recording electrodes *Annu. Rev. Biomed. Eng.* **10** 275–309
- [23] Cherubini E and Miles R 2015 The CA3 region of the hippocampus: how is it? what is it for? how does it do it? *Front Cell Neurosci.* **9** 19
- [24] Diamond M C, Johnson R E and Ingham C A 1975 Morphological changes in the young, adult and aging rate cerebral cortex, hippocampus, and diencephalon *Behav. Biol.* **14** 163–74
- [25] Sponaugle A E, Badanich K A and Kirstein C L 2008 Localization of stereotaxic coordinates for the ventral tegmental area in early adolescent, mid-adolescent and adult rats *Brain Res.* **1218** 215–23
- [26] Nahm F K D, Dale A M, Albright T D and Amaral D G 1994 In vivo microelectrode localization in the brain of the alert monkey- a combined radiographic and magnetic resonance imaging approach *Exp Brain Res.* **98** 401–11
- [27] Borg J S et al 2015 Localization of metal electrodes in the intact rat brain using registration of 3D microcomputed tomography images to a magnetic resonance histology atlas *eNeuro* **2** 0017–15
- [28] Dagdeviren C et al 2018 Miniaturized neural system for chronic, local intracerebral drug delivery *Sci. Transl. Med.* **10** eaan2742
- [29] Potter K A, Buck A C, Self W K and Capadona J R 2012 Stab injury and device implantation within the brain results in inversely multiphasic neuroinflammatory and neurodegenerative responses *J. Neural Eng.* **9** 046020